AIAA JOURNAL
Vol. 33, No. 11, November 1995

Asymmetric Elastic Buckling of Axially Compressed Conical Shells with Various End Conditions

N. Pariatmono*
BPP Teknologi, Jakarta 10340, Indonesia
and
M. K. Chryssanthopoulos†
Imperial College, London SW7 2B4, England, United Kingdom

Two different solutions to the problem of simply supported conical shells under axial compression suggested by previous investigators are extensively compared and the problems associated with each type of solution are identified. In terms of buckling load, both solutions are in good agreement but significant differences are clearly shown in buckling mode comparisons. It is also shown that in certain cases, different modes correspond to the same value of critical load. On the basis of the numerical performance of each solution, a displacement function is selected and the study is extended to investigate mode effects in cones with clamped boundary conditions. The numerical difficulties encountered in simply supported cones are reduced in this case. Clamping alters the shape of the buckling mode not only in the vicinity of the boundaries, as may be expected, but also in the center of the cone.

Nomenclature

a_m = coefficients defining buckling mode
D = bending stiffness $[Et^3/12(1-\mu^2)]$
E = modulus of elasticity
F = stress function
f = nondimensionalized form of F
L = slant length of the cone; see Fig. 1
M = number of terms used in Galerkin procedure
m = number of half-waves in meridional direction
$\bar{m}$ = modified m; see Eq. (9) for simple support and Eq. (18) for clamped support
N = number of full waves in circumferential direction
N_s = normal stress resultant in meridional direction
$N_{s\theta}$ = shear stress resultant
N_θ = normal stress resultant in circumferential direction
P = compressive load
P_{cl} = classical buckling load corresponding to axisymmetric mode; see Eq. (1)
R_1 = small radius of the cone; see Fig. 1
R_2 = large radius of the cone; see Fig. 1
s = coordinate in meridional direction measured from apex of the cone; see Fig. 1
(s_1, s_2) = value of s coordinate at small- and large-radius end, respectively; see Fig. 1
t = thickness of the cone perpendicular to the shell wall
U = displacement in meridional direction, positive toward the large radius; see Fig. 1
V = displacement in circumferential direction; see Fig. 1
W = out-of-plane displacement of the cone, positive toward symmetry axis of the cone; see Fig. 1
Z = non-dimensional geometric parameter defined in Eq. (3)
α = semivertex angle of the cone
β = modified N, $N/\sin\alpha$
γ = truncation parameter, s_1/s_2, $0 \le \gamma \le 1$
θ = circumferential coordinate
μ = Poisson's ratio
ϕ = modified circumferential coordinate θ, $\theta \sin\alpha$
$\bar{\nabla}$ = partial differential operator, see Eq. (4)

Received July 5, 1994; revison received Jan. 11, 1995; accepted for publication Jan. 11, 1995.

*Research Staff, Directorate of Engineering Science, Gedung Baru BPPT lantai 17, Jalan M. H. Thamrin 8.
†Lecturer, Department of Civil Engineering.

I. Introduction

MANY investigators have studied the behavior of conical shells under axial compression. At the early stages of the research, the studies were aimed at developing suitable governing equations to enable the presentation of nonlinear equilibrium equations analogous to the Donnell equations for cylindrical shells.[1,2]

An investigation of axisymmetric buckling revealed that the buckling load of a cone under axial compression is the same as that of a cylinder with thickness equal to the component of the cone thickness perpendicular to the longitudinal axis,[3] i.e.,

$$P_{cl} = \frac{2\pi Et^2}{\sqrt{3(1-\mu^2)}}\cos^2\alpha \tag{1}$$

Subsequent studies dealt with linearized stability equations and the solution to the asymmetric buckling problem.[4–6] In 1970, two independent works, by Tani and Yamaki[4] and by Baruch et al.,[5] provided results for buckling loads using different approaches and different types of solutions. The former started with the stability equations in F–W form and introduced a polynomial function as the assumed out-of-plane displacement W. The latter assumed that the displacements U, V, and W are given as a series containing the combination of an exponential and trigonometric function and, hence, employed a displacement formulation of the stability equations. In both cases, solutions were obtained using a Galerkin procedure. Recently, the latter approach was extended to analyze orthotropic conical shells.[6]

In this paper, the F–W method is adopted, but two different types of displacement functions are used. Results obtained are contrasted in terms of both buckling loads and buckling modes. An assessment of the two solutions is also carried out by considering the numerical performance in achieving convergence. Using the preferred solution, the study then extended to analyze axially compressed cones with clamped boundary conditions which have not been investigated in detail by previous researchers.

It is worth noting that results presented here are for asymmetric (periodic) buckling. As pointed out by Baruch et al.,[5] axisymmetric buckling can lead to lower buckling loads in cones for certain boundary conditions (simply supported out-of-plane, varying in-plane restraint).

II. Governing Equations and Boundary Conditions

Nonlinear equations for cones under axial compression have been presented by several investigators.[1,2] By applying the adjacent equilibrium principle, i.e., $U = U_0 + U_1$, $V = V_0 + V_1$ and $W = W_0 + W_1$, where subscript (0) is used for prebuckling

displacements and subscript (1) for buckling mode components, a nonlinear set of stability equations is obtained.[7] Assuming that during prebuckling the rotations can be neglected and the stresses are expressed by membrane solutions, the linear stability equations are obtained.[8] Making use of the nondimensional quantities,

$$x = \frac{s}{s_2} \qquad u = \frac{U_1}{t\cot\alpha} \qquad v = \frac{V_1}{t\cot\alpha} \qquad w = \frac{W_1}{t}$$
$$f = \frac{F_1}{Et^2 s_2 \cot\alpha} \qquad (n_s, n_\theta, n_{s\theta}) = (N_s, N_\theta, N_{s\theta})\frac{s_2}{Et^2\cot\alpha} \tag{2}$$

and the following parameters,

$$\gamma = \frac{s_1}{s_2} \qquad Z = \sqrt{\frac{Ets_2^2\cot^2\alpha}{12D}} = \frac{s_2^2}{R_2 t}\cos\alpha\sqrt{1-\mu^2}$$
$$k_c = \frac{Ps_2}{\pi D\sin 2\alpha} = \frac{Ps_2^2}{2\pi DR_2\cos\alpha} = 4\frac{P}{P_{cl}}\sqrt{3(1-\mu^2)}\frac{s_2}{t}\cot\alpha \tag{3}$$

the aforementioned stability equations can be expressed as[4,8]

$$\bar\nabla\bar\nabla f = -\frac{1}{x}w_{,xx} \tag{4a}$$

$$\bar\nabla\bar\nabla w + k_c\frac{1}{x}w_{,xx} = -12Z^2\frac{1}{x}f_{,xx} = 0 \tag{4b}$$

where

$$\bar\nabla \equiv \frac{\partial^2}{\partial x^2} + \frac{1}{x}\frac{\partial}{\partial x} + \frac{1}{x^2}\frac{\partial^2}{\partial\phi^2}$$

and

$$\phi = \theta\sin\alpha$$

Note that all symbols are defined in the Nomenclature and Fig. 1.

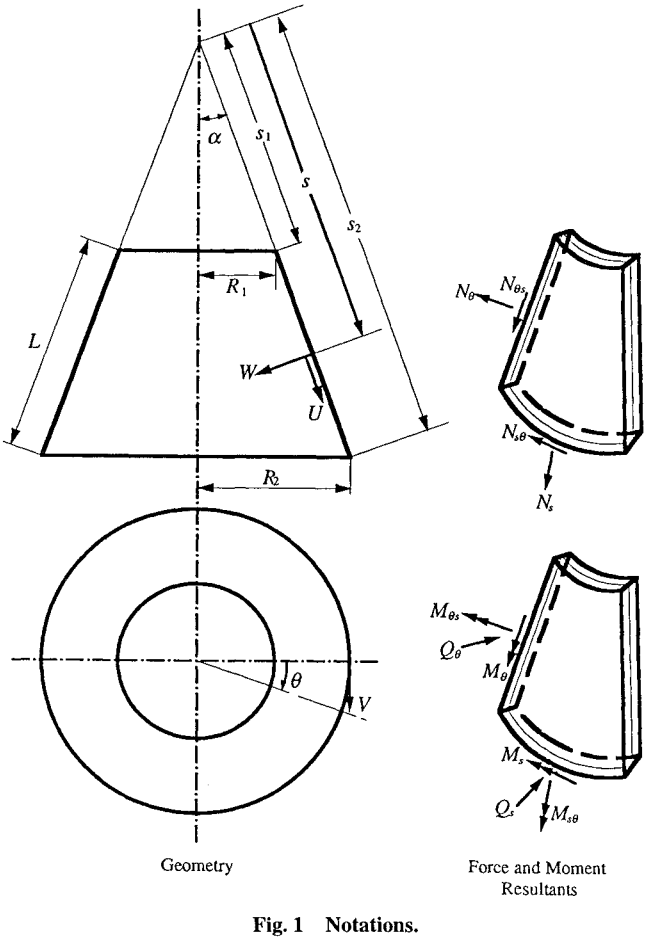

Fig. 1 Notations.

The boundary conditions consist of out-of-plane and in-plane end conditions. There are two out-of-plane conditions, i.e. simple, (SS) and clamped (CC) support, which can be formulated at $x = 1$ and $x = \gamma$ as

$$\text{SS:} \quad w = 0 \quad \text{and} \quad w_{,xx} + \frac{\mu}{x}\left(w_{,x} + \frac{1}{x}w_{,\phi\phi}\right) = 0 \tag{5a}$$

$$\text{CC:} \quad w = 0 \quad \text{and} \quad w_{,x} = 0 \tag{5b}$$

whereas the in-plane conditions consist of four combinations at $x = 1$ and $x = \gamma$:

$$n_{s\theta} = n_s = 0 \tag{6a}$$
$$n_{s\theta} = u = 0 \tag{6b}$$
$$v = n_s = 0 \tag{6c}$$
$$v = u = 0 \tag{6d}$$

Expressed in (w, f) and adopting linear theory, these in-plane parameters may be obtained from[4,7,8]

$$n_s = \frac{1}{x}\left(f_{,x} + \frac{1}{x}f_{,\phi\phi}\right) \qquad n_\theta = f_{,xx}$$
$$n_{s\theta} = \frac{1}{x}\left(\frac{1}{x}f_{,\phi} - f_{,x\phi}\right) \qquad u_{,x} = \frac{1}{x}\left(f_{,x} + \frac{1}{x}f_{,\phi\phi} - \mu x f_{,xx}\right)$$
$$v_{,\phi} = xf_{,xx} - \mu f_{,x} \qquad -\frac{\mu}{x}f_{,\phi\phi} - u + w \tag{7}$$

By combining the out-of-plane (5) and in-plane (6) conditions, there are eight sets of boundary conditions, i.e., SS-1–SS-4 and CC-1–CC-4.

III. Simply Supported Cones

As mentioned previously, two families of assumed displacement function have been proposed for solving the governing equations (4). Tani and Yamaki[4] employed a displacement function in the form

$$w = \sum_{m=0}^{M} a_m \sum_{j=0}^{4} c_{mj}x^{m+j}\cos N\theta \tag{8}$$

whereas Baruch et al.[5] used

$$w = \sum_{m=1}^{M} a_m\left(\frac{x}{\gamma}\right)^r \sin\left[\bar m\log\left(\frac{x}{\gamma}\right)\right]\sin N\theta \qquad \bar m = \frac{m\pi}{\log(1/\gamma)} \tag{9}$$

Both functions satisfy the simply supported out-of-plane boundary conditions (5a), provided that, as noted by Baruch et al.,[5] the value of the parameter r in Eq. (9) is set to $\frac{1}{2}(1-\mu)$.

In the present analysis, both types of functions are considered, and a solution is obtained by following a Galerkin procedure.[4,7,8] In the following, the Galerkin procedure used is briefly presented for the case where the displacement function is given by Eq. (9). The procedure is similar to that described by Yamaki and Tani,[8] who used a displacement function given by Eq. (8).

Substituting Eq. (9) into Eq. (4a) yields

$$\bar\nabla\bar\nabla f = \sum_{m=1}^{M} a_m\left[(\bar m^2 + r - r^2)w_1 + (\bar m - 2\bar m r)w_2\right]\frac{1}{x^3}\sin N\theta \tag{10}$$

where

$$w_1 = (x/\gamma)^r\sin[\bar m\log(x/\gamma)]$$
$$w_2 = (x/\gamma)^r\cos[\bar m\log(x/\gamma)] \tag{11}$$

The general solution for this equation is

$$f = \sum_{m=1}^{M}\left(f_{m1}x^{-\beta} + f_{m2}x^{\beta} + f_{m3}x^{-\beta+2} + f_{m4}x^{\beta+2} + d_1xw_1 + d_2xw_2\right)a_m\sin N\theta \tag{12}$$

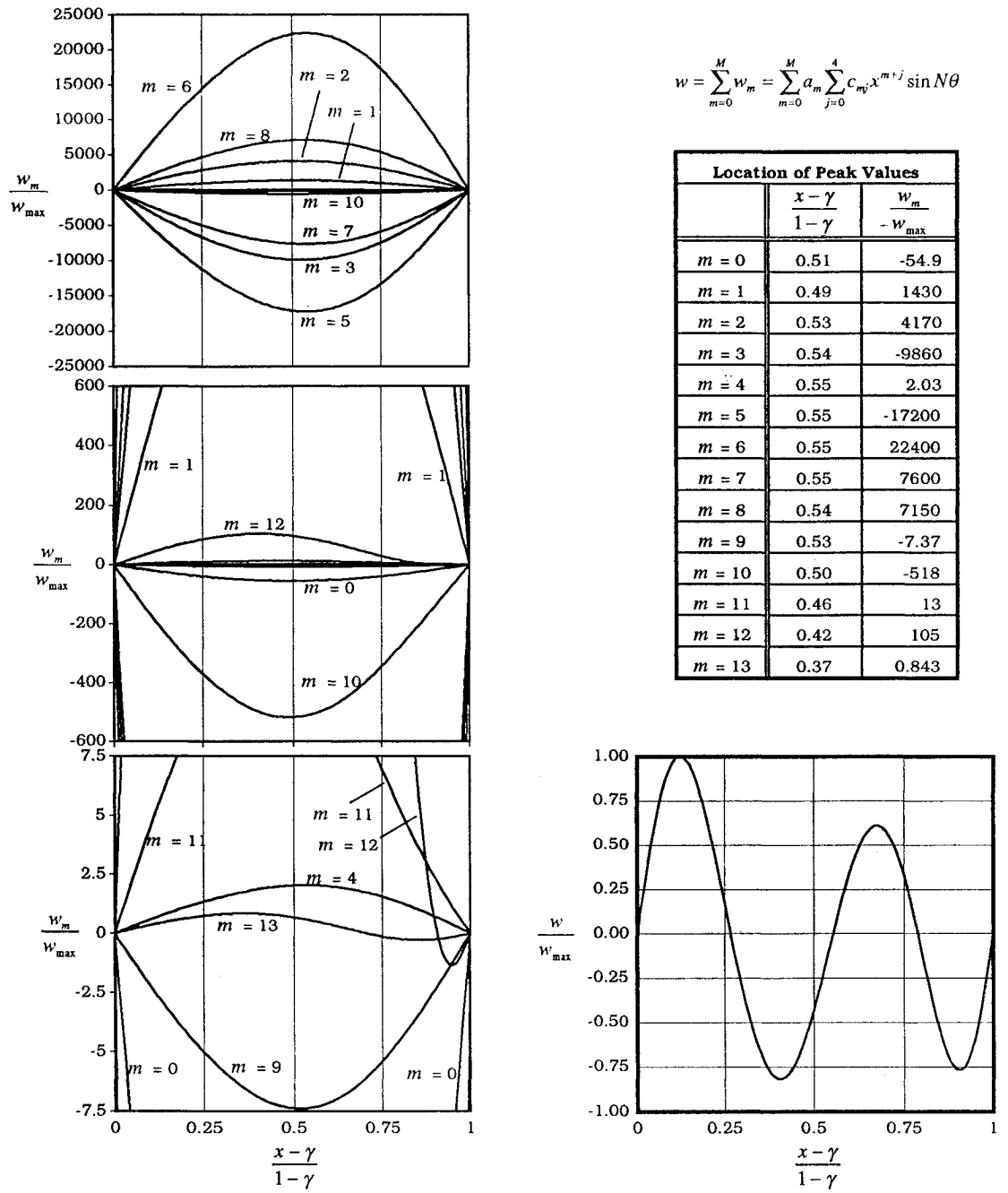

$$w = \sum_{m=0}^{M} w_m = \sum_{m=0}^{M} a_m \sum_{j=0}^{4} c_{mj} x^{m+j} \sin N\theta$$

Location of Peak Values

	$\frac{x-\gamma}{1-\gamma}$	$\frac{w_m}{w_{max}}$
$m = 0$	0.51	-54.9
$m = 1$	0.49	1430
$m = 2$	0.53	4170
$m = 3$	0.54	-9860
$m = 4$	0.55	2.03
$m = 5$	0.55	-17200
$m = 6$	0.55	22400
$m = 7$	0.55	7600
$m = 8$	0.54	7150
$m = 9$	0.53	-7.37
$m = 10$	0.50	-518
$m = 11$	0.46	13
$m = 12$	0.42	105
$m = 13$	0.37	0.843

Fig. 2 Mode decomposition for Eq. (8), simple support (BC: SS-4): $L/t = 100$, $\gamma = 0.8$, $R_1/t = 127.5$, $\alpha = 18.4$ deg, $M = 14$, $k_c = 9921$, and $P/P_{cl} = 0.9890$.

where

$$\beta = N/\sin\alpha$$

In Eq. (12) $f_{mj} (j = 1, 2, 3, 4)$ are constants to be determined from the in-plane boundary condition (6), whereas d_1 and d_2 are the solution of two simultaneous equations

$$\sum_{j=1}^{2} g_{ij} d_j = G_i \qquad i = 1, 2 \tag{13}$$

where

$$g_{11} = g_{22} = 1 + 2\bar{m}^2 + \bar{m}^4 - 2r^2 - 6\bar{m}^2 r^2 + r^4 + \beta^4 - 2\beta^2 + 2\bar{m}^2\beta^2 - 2r^2\beta^2$$

$$g_{12} = -g_{21} = 4\bar{m}r(1 + \beta^2 + \bar{m}^2 - r^2)$$

$$G_1 = \bar{m}^2 + r - r^2$$

$$G_2 = \bar{m}(1 - 2r)$$

Substituting Eq. (12) into Eq. (7) and solving for u and v, the following relations are obtained:

$$n_s = \sum_{m=1}^{M} a_m \sin N\theta \big[-\beta(\beta+1) f_{m1} x^{-\beta-2} - \beta(\beta-1) f_{m2} x^{\beta-2} - (\beta+2)(\beta-1) f_{m3} x^{-\beta} - (\beta-2)(\beta+1) f_{m4} x^{\beta} - d_1(1/x)\{(\beta^2 - r - 1)w_1 - \bar{m}w_2\} - d_2(1/x)\{\bar{m}w_1 + (\beta^2 - r - 1)w_2\}\big] \tag{14a}$$

$$n_{s\theta} = \sum_{m=1}^{M} a_m \cos N\theta \big[\beta(\beta+1) f_{m1} x^{-\beta-2} - \beta(\beta-1) f_{m2} x^{\beta-2} + \beta(\beta-1) f_{m3} x^{-\beta} - \beta(\beta+1) f_{m4} x^{\beta} - d_1(1/x)\beta(rw_1 + \bar{m}w_2) + d_2(1/x)\beta(\bar{m}w_1 + rw_2)\big] \tag{14b}$$

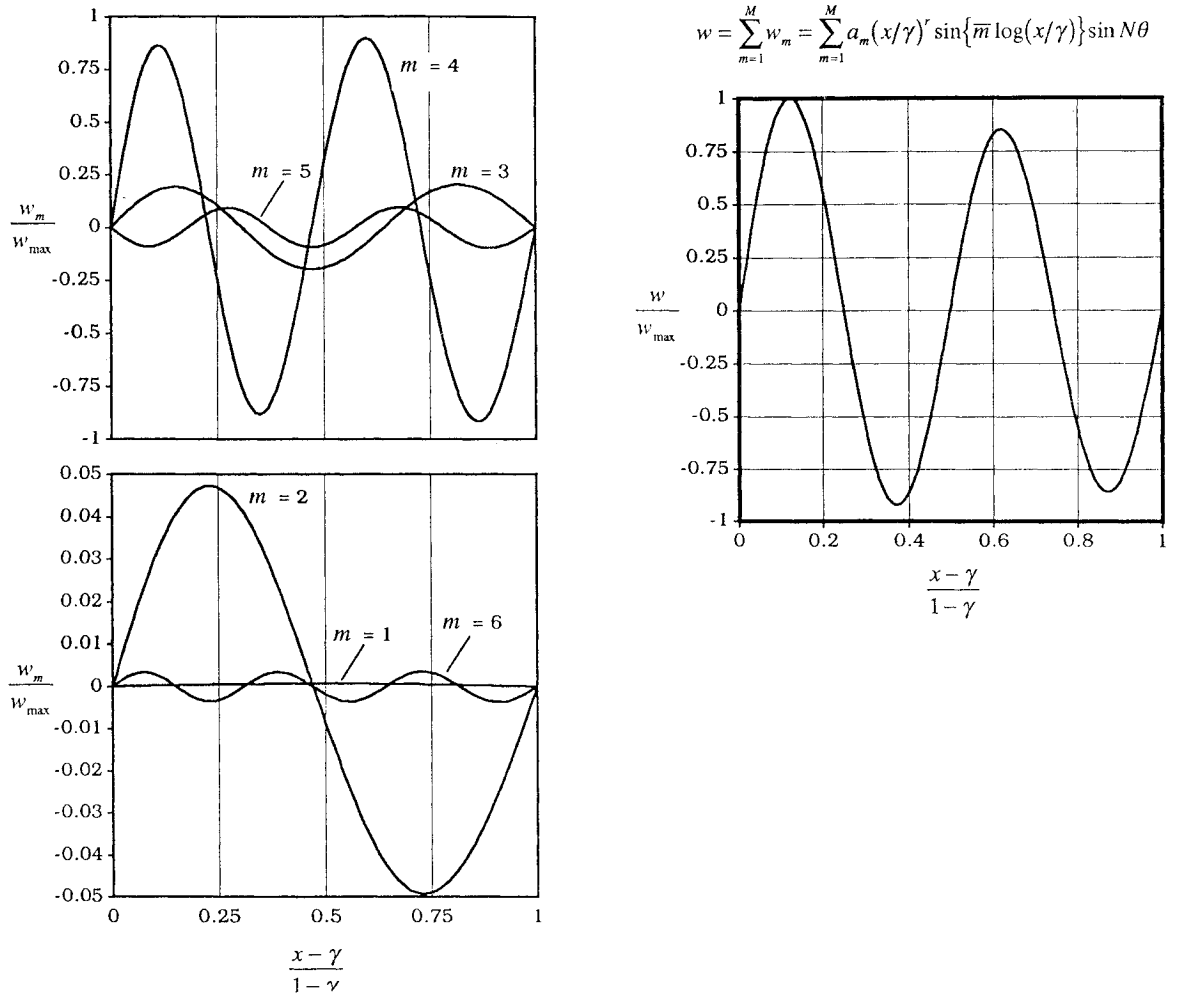

Fig. 3 Mode decomposition for Eq. (9), simple support (BC: SS-4): $L/t = 100$, $\gamma = 0.8$, $R_1/t = 127.5$, $\alpha = 18.4$ deg, $M = 6$, $k_c = 9920$, and $P/P_{cl} = 0.9889$.

$$u = \sum_{m=1}^{M} a_m \sin N\theta\big[\beta(1+\mu)f_{m1}x^{-\beta-1} - \beta(1+\mu)f_{m2}x^{\beta-1} + \{\beta(1+\mu)+2(1-\mu)\}f_{m3}x^{-\beta+1} - \{\beta(1+\mu)-2(1-\mu)\}f_{m4}x^{\beta+1} + d_1w_1(-k_1r - k_2\bar{m}) + d_1w_2(k_1\bar{m} - k_2r) + d_2w_1(k_2r - k_1\bar{m}) + d_2w_2(-k_2\bar{m} - k_1r)\big] \quad (14c)$$

$$v = \sum_{m=1}^{m} a_m \cos N\theta\big[-\beta(1+\mu)f_{m1}x^{-\beta-1} - \beta(1+\mu)f_{m2}x^{\beta-1} - (\beta+\beta\mu-4)f_{m3}x^{-\beta+1} - (\beta+\beta\mu+4)f_{m4}x^{\beta+1} + d_1(l_1w_1 + l_2w_2) - d_2(l_2w_1 - l_1w_2) - w_1/\beta\big] \quad (14d)$$

where

$$(k_1, k_2) = \frac{[\{-1+\beta^2-\bar{m}^2\mu - r + \mu r + \mu r^2\}, \{\bar{m}(-1+\mu+2\mu r)\}]}{\bar{m}^2 + r^2}$$

$$l_1 = \left(-k_2\bar{m} + \bar{m}^2 + \mu - \beta^2\mu - r - k_1r + \mu r - r^2\right)/\beta$$

$$l_2 = \left(-\bar{m} + k_1\bar{m}^2 + \bar{m}\mu - k_2r - 2\bar{m}r\right)/\beta$$

Using Eq. (14) and the in-plane boundary conditions (6), the coefficients $f_{mj}(j = 1, 2, 3, 4)$ can be determined for each type of simple support (SS-1–SS-4). At this stage, the expressions for w and f satisfy the boundary and compatibility conditions exactly. The remaining governing equations (4b) is solved using the Galerkin method, which leads to

$$\int_0^{2\pi}\int_\gamma^1 \left[\bar{\nabla}\bar{\nabla}w + k_c\frac{1}{x}w_{,xx} - 12Z^2\frac{1}{x}f_{,xx}\right]\left(\frac{x}{\gamma}\right)^r \times \sin\left[\bar{n}\log\left(\frac{x}{\gamma}\right)\right]\sin N\theta\, dx\, d\theta = 0$$

$$\bar{n} = n\pi/\log(1/\gamma) \qquad n = 1, 2, \ldots, M \quad (15)$$

Substituting Eqs. (9) and (12) into Eq. (15) the following system of equations in the unknown coefficients $a_m(m = 1, 2, \ldots, M)$ is finally obtained:

$$\boldsymbol{Aa} + k_c\boldsymbol{Ba} - 12Z^2\boldsymbol{Ca} = \boldsymbol{0} \quad (16)$$

where the elements of matrices $\boldsymbol{A}$, $\boldsymbol{B}$, and $\boldsymbol{C}$ of dimension $M \times M$ are given by

$$A_{nm} = \int_\gamma^1 \bar{\nabla}\bar{\nabla}\left[\left(\frac{x}{\gamma}\right)^r \sin\left\{\bar{m}\log\left(\frac{x}{\gamma}\right)\right\}\right] \times \left(\frac{x}{\gamma}\right)^r \times \sin\left\{\bar{n}\log\left(\frac{x}{\gamma}\right)\right\} dx$$

$$B_{nm} = \int_\gamma^1 \frac{1}{x}\left[\left(\frac{x}{\gamma}\right)^r \sin\left\{\bar{m}\log\left(\frac{x}{\gamma}\right)\right\}\right]_{,xx} \times \left(\frac{x}{\gamma}\right)^r \times \sin\left\{\bar{n}\log\left(\frac{x}{\gamma}\right)\right\} dx$$

Table 1 Comparison with Tani and Yamaki[4] for simple support and $L/t = 100$

Parameters					Value of buckling load parameter k_c[a]		
	Z[b]	α, deg	Boundary conditions	N	Tani and Yamaki	Present, Eq. (8)	Present, Eq. (9)
	11.92	84.3	SS-1	1	44.01	44.02 {6}[c]	44.42 {11}
			SS-4	1	81.43	81.61 {5}	81.67 {6}
γ[d] $= 0.2$	17.89	81.5	SS-1	1	67.58	67.58 {7}	68.05 {11}
			SS-4	2	124.7	126.1 {4}	126.1 {5}
	59.62	63.4	SS-1	1	213.6	212.4 {10}	212.5 {17}
			SS-4	3	413.1	413.9 {6}	425.5 {4}
	38.16	78.7	SS-1	1	129.1	129.1 {5}	129.3 {8}
			SS-4	2	263.5	263.7 {4}	263.8 {4}
$\gamma = 0.5$	57.24	73.3	SS-1	1	205.9	205.9 {5}	206.2 {8}
			SS-4	5	397.6	397.6 {5}	397.8 {4}
	190.8	45.0	SS-1	1	664.7	672.4 {11}	666.3 {12}
			SS-4	8	1321	1346 {4}	1338 {6}
	143.1	73.3	SS-1	1	428.0	427.9 {5}	434.7 {2}
			SS-4	9	999.3	999.3 {3}	999.1 {3}
	286.2	59.0	SS-1	1	951.2	952.1 {11}	1058 {2}
$\gamma = 0.8$			SS-4	6	1984	1993 {3}	1984 {4}
	429.3	48.0	SS-1	1	1533	1540 {19}	1557 {4}
			SS-4	11	2977	2982 {3}	2975 {4}
	1431	18.4	SS-1	1	4971	5333 {24}	5185 {6}
			SS-4	8	9919	9921 {14}	9920 {6}

[a] $k_c = Ps_2/\pi D \sin 2\alpha$. [b] $Z = (s_2^2/R_2 t)\cos\alpha\sqrt{(1-\nu^2)}$. [c] Number of terms needed to achieve convergence in braces.
[d] $\gamma = s_1/s_2$.

$$C_{nm} = \int_{\gamma}^{1} \frac{1}{x}\left[f_{m1}x^{-\beta} + f_{m2}x^{\beta} + f_{m3}x^{-\beta+2} + f_{m4}x^{\beta+2} + d_1 x w_1 + d_2 x w_2\right]_{,xx} (x/\gamma)^r \sin\{\bar{n}\log(x/\gamma)\}\,dx$$

$$\bar{n} = n\pi/\log(1/\gamma) \qquad n = 1, 2, \ldots, M \tag{17}$$

Equation (16) forms a general eigenvalue problem with the load parameter k_c acting as eigenvalue and the unknown coefficients a_m as eigenvectors.

Following the given procedure, the results are obtained and the comparison with Tani and Yamaki[4] is shown in Table 1. It is worth noting, however, that some of the geometries have rather extreme properties ($\alpha > 80$ deg) and, in this respect, the validity of the equations used may be questionable. However, the cases given by Tani and Yamaki[4] are included here for validation purposes.

To produce directly comparable results, the number of circumferential waves is set equal to the number given by Tani and Yamaki.[4] As can be seen in Table 1, comparison is generally very good, especially for low values of Z and large semivertex angle α, but somewhat worse for high Z and small α. In addition, the expression (9) suggested by Baruch et al.[5] has also been used and, as shown, gives very good results in all cases.

By examining other combinations of in-plane conditions, it is also possible to compare the results with those obtained by Baruch et al.[5] The comparison is presented in Table 2. The parameter P/P_{cl} shown in these tables is the buckling load obtained using the Galerkin method divided by the classical buckling load given by Eq. (1). Note that examples from Ref. 5 cover a wide range of α values, from a near cylindrical to a highly conical geometry.

The difficulty in finding eigenvalues for cones with small α and high value of Z is again revealed when the polynomial (8) is used. Discrepancies are generally more pronounced for long cones. Further, as the number of terms used in Eq. (8) increases, the matrices involved in the general eigenvalue problem become ill conditioned.[9] This encourages the use of a deflection function of the form given by Eq. (9), which combines exponential and trigonometric functions. This type of function assures convergence (defined here, as can be seen from Tables 1 and 2, to four significant digits), although in some cases, the number of terms needed to achieve convergence using Eq. (9) is larger than that using Eq. (8).

Attention is now drawn to the buckling mode, so that results obtained can be assessed in more detail. In Fig. 2, the terms that build up the polynomial given by Eq. (8) are shown for a typical geometry. The individual polynomial terms of Eq. (8) are plotted on the three charts shown on the left using an appropriate amplitude scale, and the most dominant terms are shown at the top. As can be seen, the polynomial function consists mainly of single half-wave modes with very large amplitude. The peaks of these modes, however, are not coincident with each other with respect to the meridional coordinate (see table of peak values on the right). Hence, after summation the final mode consists of four half-waves as shown on the right.

In contrast, the individual terms of Eq. (9) contain a number of axial waves and are all quite similar to the final mode produced after superposition (see Fig. 3). The ability of this function to generate sinusoidal waves with varying wavelength reduces the number of terms needed to produce the final mode and, hence, convergence can be achieved more rapidly.

The other important difference between polynomial and sinusoidal functions is related to the amplitude of individual modes. Whereas the final mode of expression (9) has an amplitude of the same order as its dominant component (in this case, $m = 4$), the summation of individual modes of Eq. (8) produces an amplitude for the final mode, which is 20,000 times smaller than its corresponding dominant term (in this case, $m = 6$). This huge difference in amplitude, in general, makes Eq. (8) very sensitive to numerical round-off error and subject to ill-conditioning problems.

It should be noted here that the similarity in the final mode obtained by the functions is not normally achieved. For example, Fig. 4 shows a mode comparison for some of the other cases given in Table 1. As can be seen, although the predicted buckling loads are quite similar, the corresponding modes differ substantially. It should be mentioned that the critical loads correspond to the same circumferential wave number, and that the difference between the modes obtained from Eqs. (8) and (9) arises in the axial profiles, as shown in Fig. 4. Although this could indicate the presence of near-coincident modes, it has been verified that this is not the case here, at least insofar as SS-1 conditions are concerned, by computing the second eigenvalue for the same circumferential number. As for SS-4 conditions, the second eigenvalue from both Eqs. (8) and (9) is very close to the first one, and this is further discussed later in the light of additional results.

In view of the comments made earlier regarding the performance of Eq. (8), it is believed that Eq. (9) offers a better platform from which observations about the buckling behavior of conical shells can be made.

However, apart from the buckling mode problem just discussed, good agreement between the solutions using Eqs. (8) and (9) has

Table 2 Comparison with Baruch et al.[5] for simple support and $R_1/t = 100$

Parameters						P/P_{cl}		
L/t	γ	Z	α, deg	Boundary conditions	N	Baruch et al.	Present, Eq. (8)	Present, Eq. (9)
	0.9983	1,255,000	0.5	SS-2	2	0.5104	11.22 {6}[a]	0.5116 {2}
				SS-4	7	1.005	**[b]	1.005 {2}
	0.9965	314,200	1.0	SS-2	2	0.5106	0.5681 {6}	0.5119 {2}
				SS-4	7	1.005	**	1.005 {2}
	0.9931	78,820	2.0	SS-2	2	0.5112	**	0.5124 {2}
				SS-4	7	1.005	**	1.005 {2}
20	0.9829	12,730	5.0	SS-2	2	0.5133	0.5128 {4}	0.5145 {2}
				SS-4	7	1.006	0.9692 {17}	1.006 {2}
	0.9664	3,224	10	SS-2	2	0.5184	0.5201 {4}	0.5198 {2}
				SS-4	7	1.007	1.008 {6}	1.007 {2}
	0.9091	363.5	30	SS-2	2	0.5696	0.8314 {10}	0.5696 {4}
				SS-4	7	1.017	1.017 {6}	1.017 {2}
	0.8524	74.61	60	SS-2	2	0.8924	0.9605 {3}	0.8926 {3}
	0.8354	20.44	80	SS-2	7	2.447	2.424 {4}	2.448 {3}
	0.9957	1,258,000	0.5	SS-2	2	0.5190	**	0.5206 {6}
				SS-4	8	1.002	**	1.002 {3}
	0.9913	315,900	1.0	SS-2	2	0.5191	**	0.5194 {8}
				SS-4	8	1.002	**	1.002 {2}
	0.9828	79,640	2.0	SS-2	2	0.5193	0.8078 {11}	0.5192 {10}
				SS-4	8	1.002	0.8771 {8}	1.002 {3}
50	0.9582	13,060	5.0	SS-2	2	0.5196	0.8026 {5}	0.5195 {14}
				SS-4	8	1.002	1.079 {8}	1.002 {3}
	0.9201	3,386	10	SS-2	2	0.5203	0.7825 {3}	0.5203 {16}
				SS-4	8	1.002	1.006 {8}	1.001 {3}
	0.8000	413.1	30	SS-2	2	0.5203	**	0.5199 {24}
				SS-4	7	1.001	1.003 {7}	1.001 {4}
	0.6973	91.132	60	SS-2	2	0.4657	0.4658 {6}	0.4655 {23}
				SS-4	7	1.044	1.044 {7}	1.043 {3}
	0.6701	25.49	80	SS-2	2	0.5984	0.5983 {3}	0.5983 {15}
				SS-4	3	1.015	1.015 {3}	1.016 {3}

[a]Number of terms needed to achieve convergence indicated in braces. [b]Cases where convergence has not been reached for up to 40 terms.

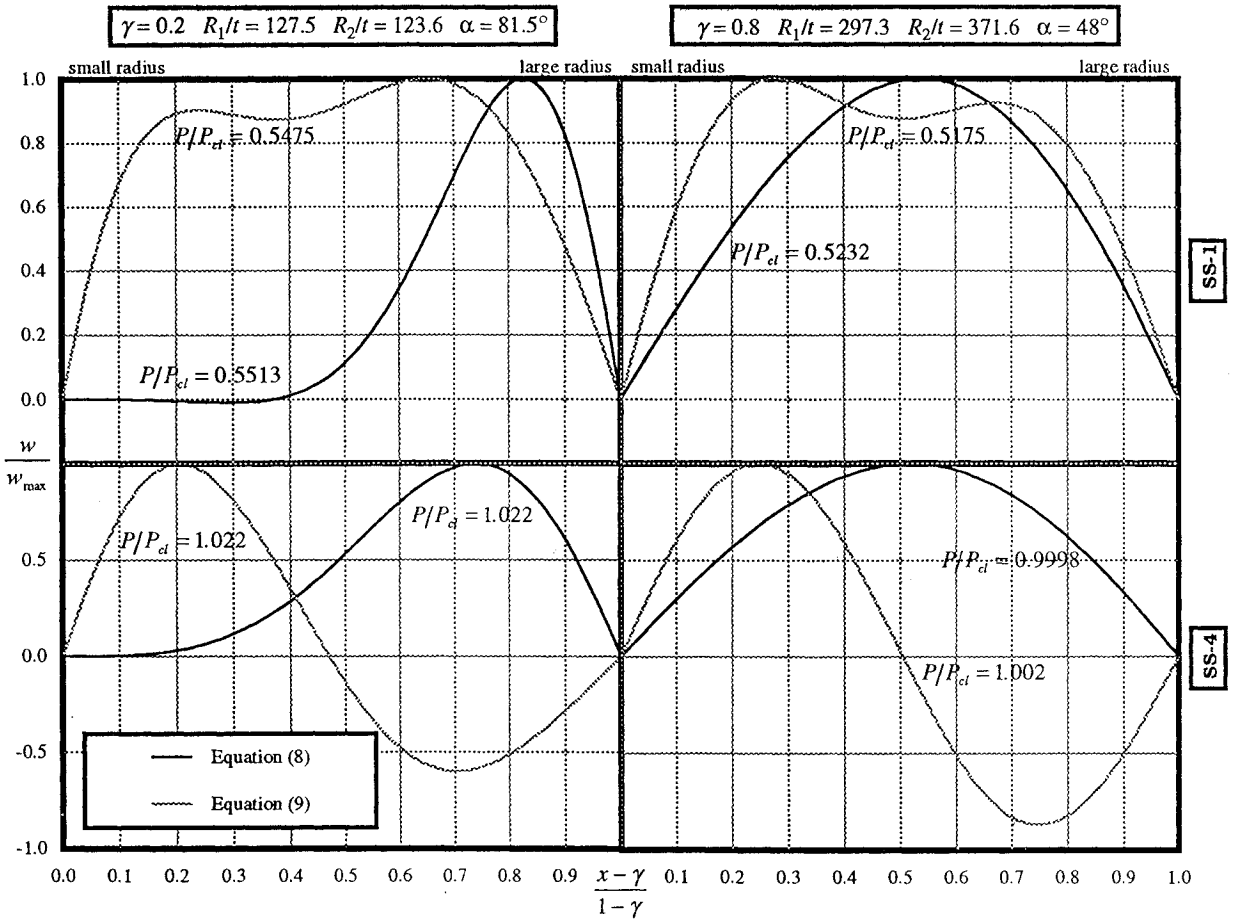

Fig. 4 Mode comparison, simple support.

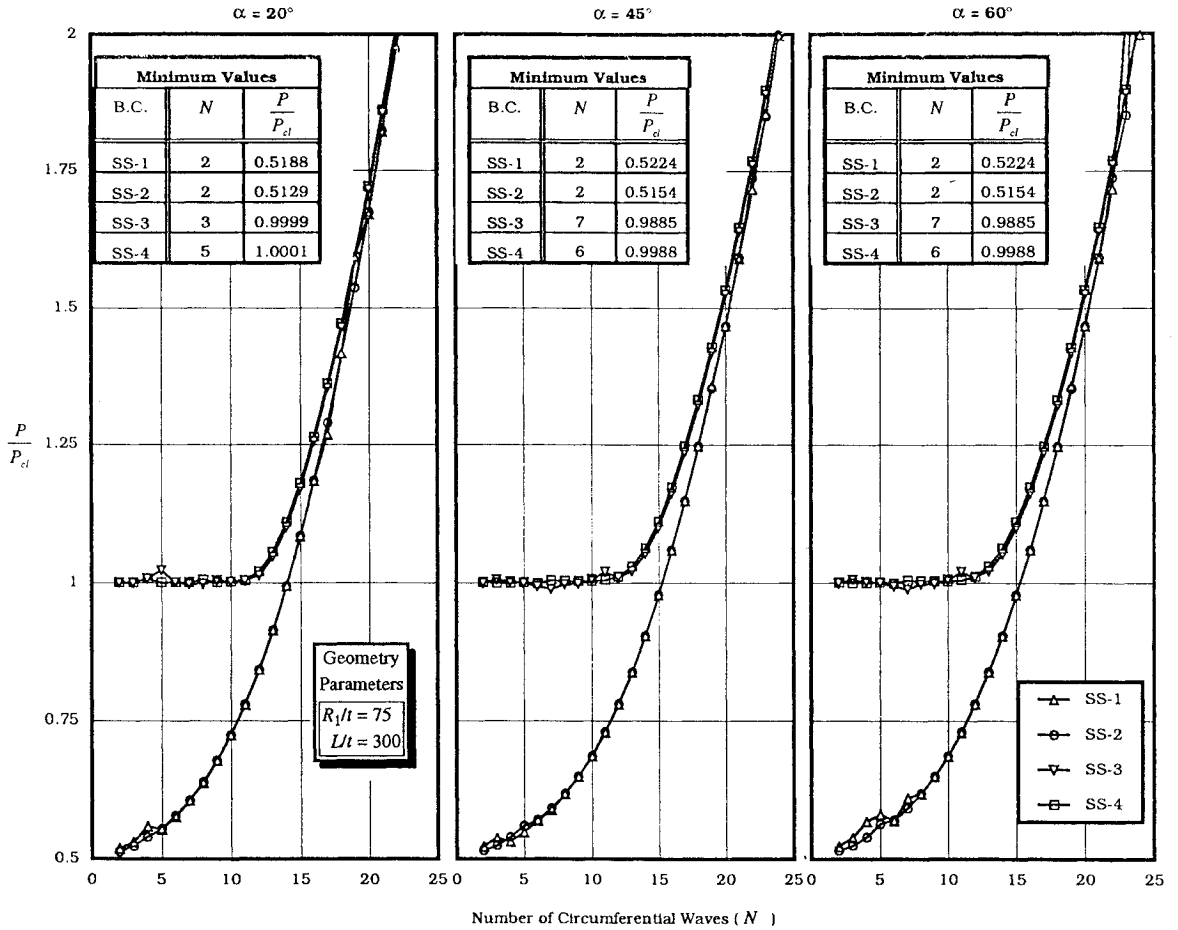

Fig. 5 Buckling load vs circumferential wave number.

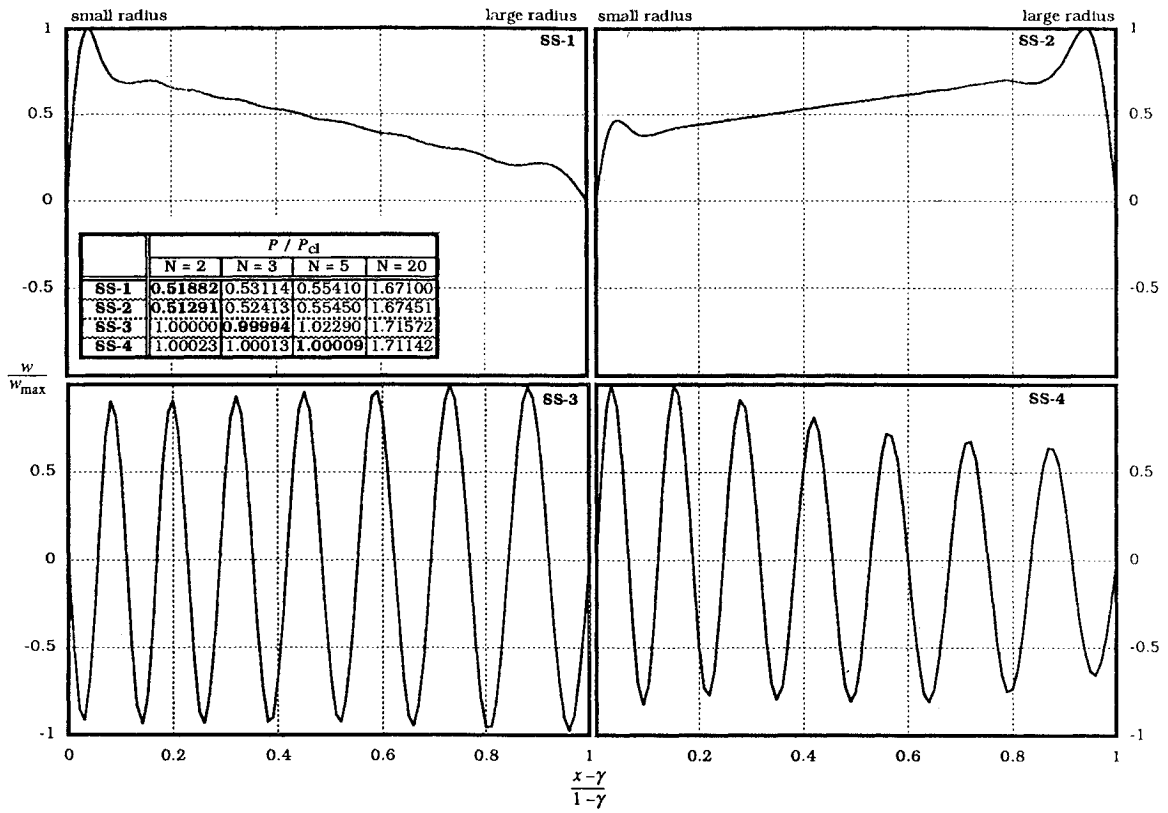

Fig. 6 Influence of boundary conditions on buckling modes. Geometry: $R_1/t = 75$, $L/t = 300$, and $\alpha = 20$ deg.

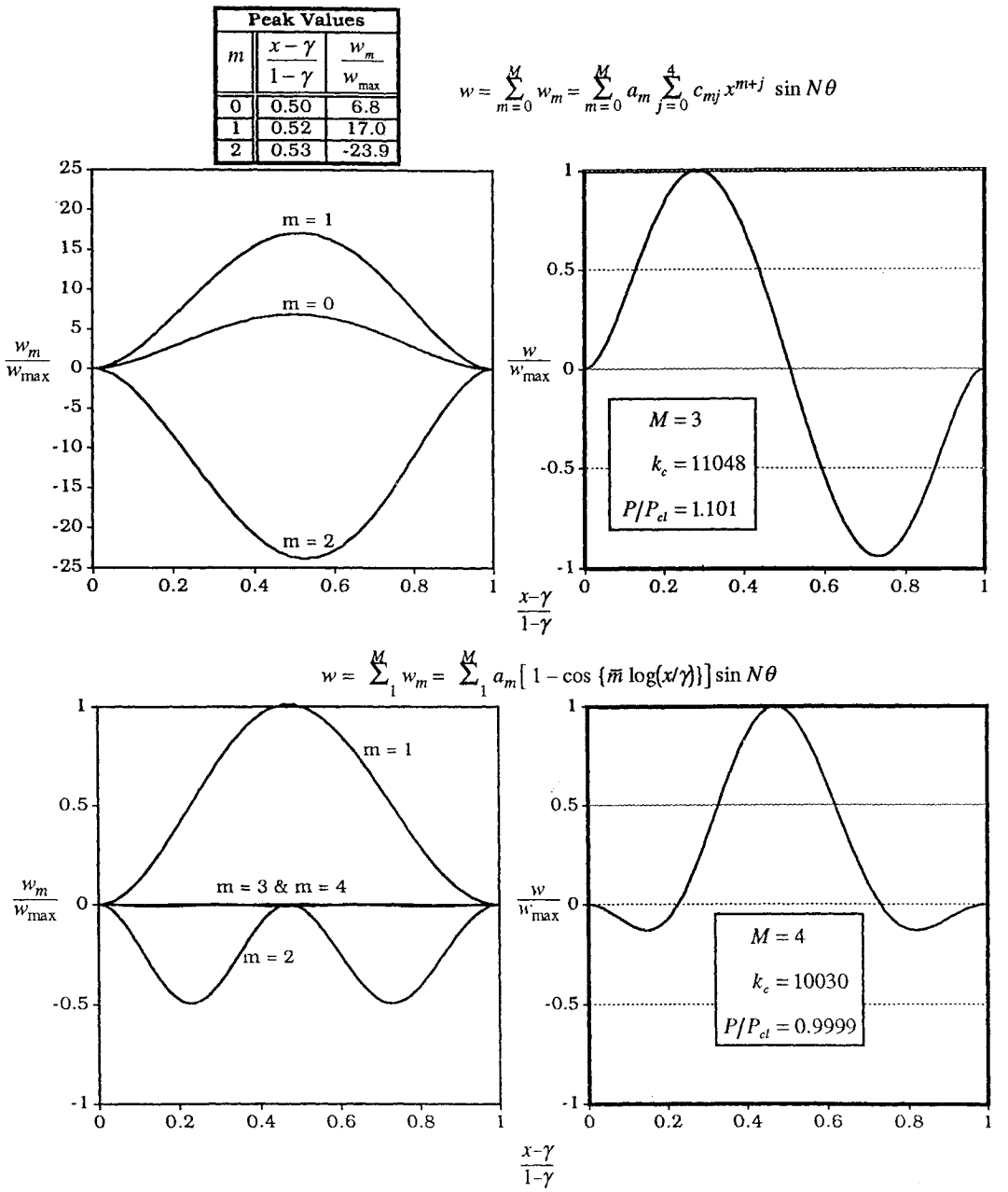

Fig. 7 Mode decomposition, clamped support (BC: CC ± 4): $L/t = 100$, $\gamma = 0.8$, $R_1/t = 127.5$, and $\alpha = 18.4$ deg.

been found in terms of buckling load as can be seen in Tables 1 and 2, and this in line with conclusions reached in earlier studies. It is worth noting the factor of 0.5 when the circumferential displacement is released at the boundaries (SS-1 and SS-2), a result that has long been recognized in cylindrical shells.[10,11]

In Fig. 5, the results of a short parameter study are presented with the aim of providing information on the critical buckling modes of simply supported conical shells. As can be seen, the lowest buckling loads seem to be equal to the classical buckling load for SS-3/SS-4 and half of that value for SS-1/SS-2. The buckling load for $N = 1$, which corresponds to column-type buckling, is not reported here as the Donnell theory is not appropriate for this case.[12] The flat part of the curve for SS-3/SS-4 conditions points to the existence of multimode solutions being admitted at the critical load similar to the well-known result for cylindrical shells. The inset table shows that for conditions SS-1 and SS-2 the value for N that gives the minimum buckling load is, however, uniquely determined in contrast to its SS-3/SS-4 counterpart. A further interesting observation may be made by concentrating on the results shown for SS-1 and SS-2 conditions. Whereas in cylindrical shells the latter leads to marginally higher critical loads than the former for the same value of N, the reverse appears to be the case for conical shells. The difference is actually very small (less than 1.5%) and, in fact, reduces as the tapering angle gets smaller, thus, moving in the direction dictated by the trend present in cylinders.

In Fig. 6, the buckling modes of a cone with various in-plane boundary conditions are plotted. The corresponding buckling loads are tabulated on the top left chart and the bold type face is used to indicate the minimum value. It may be observed that SS-1/SS-2 and SS-3/SS-4, which correspond to restrained and unrestrained circumferential movement during buckling, respectively, form pairs of similar results with approximately equal buckling load and similar buckling mode.

Furthermore, it is of interest to note the modulated amplitude of the multiwave axial profile obtained for SS-3/SS-4 conditions and to contrast it with the much flatter profile (but with stronger influence of edge effects) found for SS-1/SS-2 conditions. This is further evidence that with SS-3/SS-4 in-plane conditions, the conical shells behave in a fashion similar to their cylindrical counterparts, whereas with SS-1/SS-2 conditions the situation is radically different.

IV. Analysis of Clamped Support

For a cone with clamped boundary conditions, the procedure described earlier is followed. Equation (8) proposed by Tani and

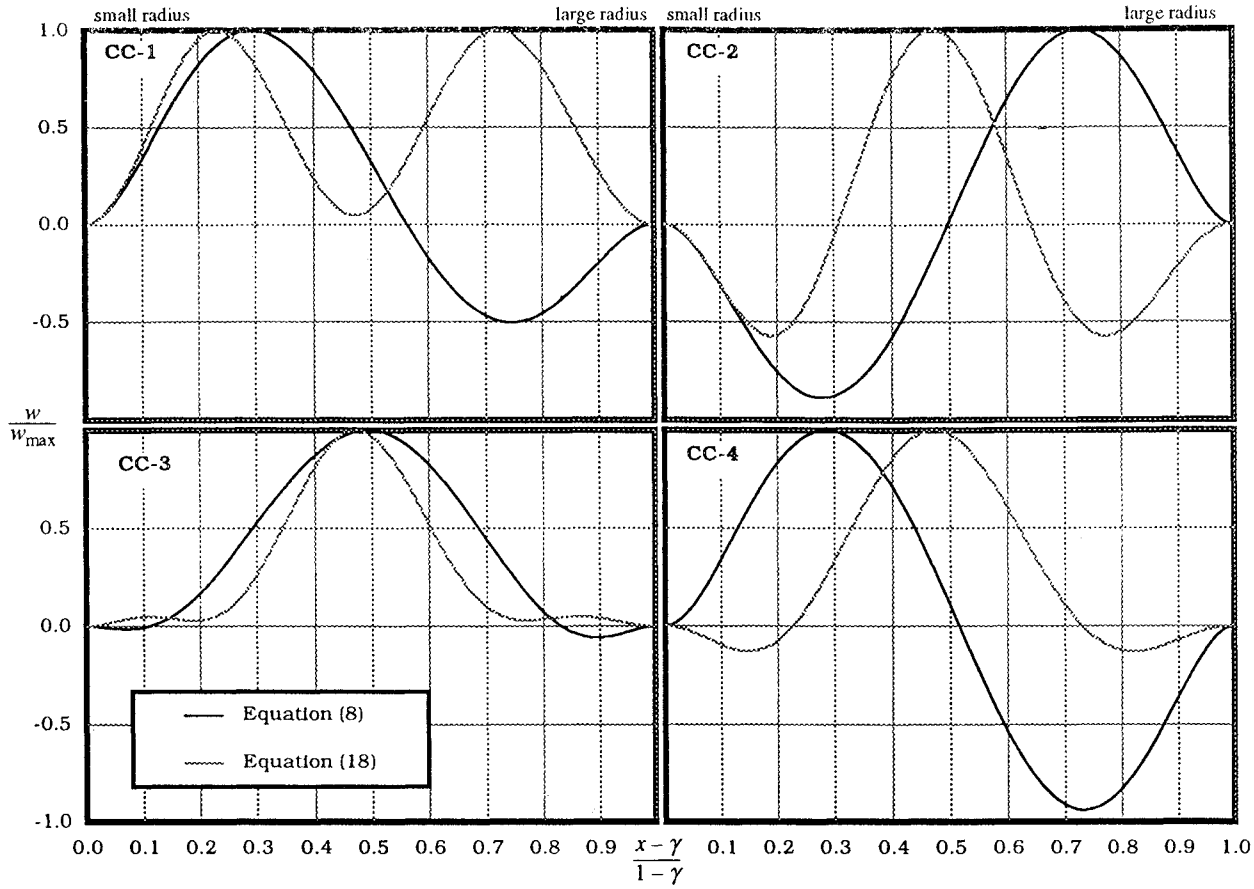

Fig. 8 Mode comparison, clamped boundary conditions. Geometry: $L/t = 100$, $R_1/t = 127.5$, and $\alpha = 18.4$ deg.

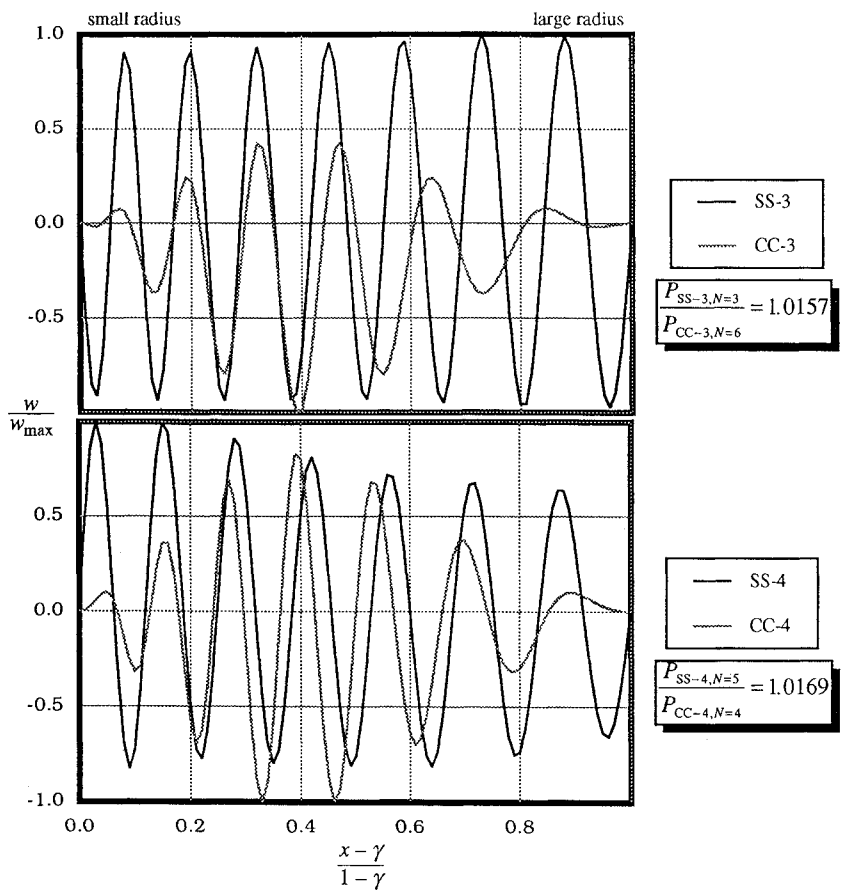

Fig. 9 Mode comparison between SS-3/CC-3 and SS-4/CC-4. Geometry: $L/t = 300$, $R_1/t = 75.0$, and $\alpha = 20$ deg.

Table 3 Comparison with Tani and Yamaki[4] for clamped support and $L/t = 100$

Parameters					Value of buckling load parameter k_c[a]		
	Z[b]	α, deg	Boundary conditions	N	Tani and Yamaki	Present, Eq. (8)	Present, Eq. (9)
	11.92	84.3	CC-1	1	82.98	82.98 {5}[c]	91.06 {5}
			CC-4	2	104.0	104.1 {5}	109.4 {3}
γ[d] = 0.2	17.89	81.5	CC-1	1	125.4	125.4 {6}	133.4 {5}
			CC-4	2	145.0	145.1 {6}	149.7 {5}
	59.62	63.4	CC-1	3	413.6	414.0 {7}	437.2 {6}
			CC-4	4	430.0	430.5 {11}	437.5 {5}
	38.16	78.7	CC-1	2	264.5	264.5 {4}	271.0 {4}
			CC-4	4	330.6	330.3 {6}	332.2 {6}
$\gamma = 0.5$	57.24	73.3	CC-1	4	399.1	399.1 {4}	403.1 {4}
			CC-4	5	463.5	463.6 {9}	463.3 {7}
	190.8	45.0	CC-1	7	1323	1324 {6}	1359 {4}
			CC-4	7	1368	1377 {7}	1353 {4}
	143.1	73.3	CC-1	1	1165	1167 {7}	1175 {3}
			CC-4	8	1521	1523 {5}	1528 {6}
	286.2	59.0	CC-1	6	1983	1982 {12}	1989 {2}
$\gamma = 0.8$			CC-4	12	2457	2466 {6}	2460 {7}
	429.3	48.0	CC-1	10	2976	2978 {4}	2982 {3}
			CC-4	9	3595	3759 {6}	3666 {7}
	1431	18.4	CC-1	7	9910	10909 {3}	9955 {4}
			CC-4	10	10240	11048 {3}	10030 {4}

[a] $k_c = Ps_2/\pi D \sin 2\alpha$. [b] $Z = (s_2^2/R_2 t)\cos\alpha\sqrt{(1-\nu^2)}$. [c] Number of terms needed to achieve convergence in braces.
[d] $\gamma = s_1/s_2$.

Yamaki[4] still can satisfy boundary condition (5b). To accommodate these out-of-plane conditions, however, Eq. (9) has to be modified to

$$w = \sum_{m=1}^{M} a_m \left[1 - \cos\left\{\bar{m}\log\left(\frac{x}{\gamma}\right)\right\}\right]\sin N\theta \qquad \bar{m}\frac{2m\pi}{\log(1/\gamma)} \tag{18}$$

Comparison with results by Tani and Yamaki[4] is shown in Table 3. The geometries are the same as those listed in Table 1 and, hence, the same comment applies here. As might be expected, the effect of damping is much more significant when combined with weak (SS-1/CC-1) rather than strong (SS-4/CC-4) in-plane conditions. Hence, the factor 0.5 previously shown in the weak simple support case (SS-1/SS-2) seems to disappear here.

In terms of numerical performance, by separating the modes into their components and comparing with Figs. 2 and 3, Fig. 7 shows that with clamped boundary conditions the difficulty in convergence has been reduced, especially when the polynomial (8) is used.

Figure 8 presents a comparison similar to that shown in Fig. 4. The difference in the buckling modes arising from the use of the two displacement functions is not as dramatic as in the simple support case. Comparison between different CC condition reveals that, although the shapes can be somewhat different, the number of waves is relatively constant for all types of CC boundary conditions.

Figure 9 contrasts the modes corresponding to simple support (SS-3 and SS-4) and clamped (CC-3 and CC-4) boundary conditions. As can be seen, the geometry chosen is one for which the effect of fixing on the buckling load is almost negligible. However, from the mode point of view, it can be observed that clamping has the effect of shifting the region of maximum amplitude from near the ends toward the center of the cone.

V. Conclusion

As a result of this investigation, a number of cases have been presented in an attempt to show geometry and boundary conditions influence on the buckling behavior of conical shells. Problems associated with selecting displacement functions have been illustrated, and suggestions on appropriate expressions have been made. Using functions that perform well numerically, it has been shown that for some geometries and boundary conditions multiple modes exist corresponding to the critical buckling load. Furthermore, an investigation on cones with clamped supports has been made. It is important to note the significant variations obtained in terms of buckling mode depending both on in-plane and out-of-plane boundary conditions. These variations should be borne in mind in tolerance specification, which is an important component in developing shell buckling guidelines.

The methodology and the results presented in this paper provide an insight into the buckling behavior of conical shells, which could also be helpful in selecting and validating appropriate numerical (finite element) models. Furthermore, the suggested procedure can be used in parametric studies to produce a set of results for design use. Whereas finite element or other specialized numerical techniques could be employed for this purpose, it is believed that analytical solutions, where available, offer advantages in terms of computational efficiency and in exposing the influence of various parameters (geometry, boundary conditions) on the predicted critical load and mode.

References

[1] Mushtari, K. M., and Galimov, K. Z., *Non-Linear Theory of Thin Elastic Shells*, Tatknigoizdat, Kanan, translated into English by J. Morgenstern and J. J. Schorr-Kon, 1957.

[2] Seide, P., "A Donnell Type Theory for Asymmetrical Bending and Buckling of Thin Conical Shells," *Journal of Applied Mechanics*, Vol. 24, pp. 547–552.

[3] Seide, P., "Axisymmetrical Buckling of Circular Cones under Axial Compression," *Journal of Applied Mechanics*, Vol. 23, No. 4, 1956, pp. 625–628.

[4] Tani, J., and Yamaki, N., "Buckling of Truncated Conical Shells under Axial Compression," *AIAA Journal*, Vol. 8, No. 3, 1970, pp. 568–571.

[5] Baruch, M., Harari, O., and Singer, J., "Low Buckling Loads of Axially Compressed Conical Shells," *Journal of Applied Mechanics*, Vol. 37, 1970, pp. 384–392.

[6] Tong, L., Tabarrok, B., and Wang, T. K., "Simple Solutions for Buckling of Orthotropic Conical Shells," *International Journal of Solids Structures*, Vol. 29, No. 8, 1992, pp. 933–946.

[7] Pariatmono, "The Collapse of Axially Compressed Conical Shells," Ph.D. Thesis, Univ. of London, London, England, 1994.

[8] Yamaki, N., and Tani, J., "Buckling of Truncated Conical Shells under Torsion," *Zeitschrift fur Angewandte Mathematik und Mechanik (ZAMM)*, Vol. 49, No. 8, 1969, pp. 471–480.

[9] Fletcher, G. A. J., *Computational Galerkin Methods*, Springer–Verlag, Berlin, 1984.

[10] Hoff, N. J., "Buckling of Thin Shells," *Proceeding of an Aerospace Scientific Symposium of Distinguished Lecturers in Honour of Theodore von Kármán on his 80th Anniversary*, Inst. of the Aerospace Sciences, New York, 1961, pp. 1–86.

[11] Arbocz, J., and Babcock, C. D., "The Effect of General Imperfections on the Buckling of Cylindrical Shells," *Journal of Applied Mechanics*, Vol. 36, 1969, pp. 28–38.

[12] Brush, D. O., and Almroth, B. O., *Buckling of Bars, Plates and Shells*, McGraw–Hill, New York, 1975.